APL Materials

Doping dependence of the electron spin diffusion length in germanium

Cite as: APL Mater. **7**, 101122 (2019); https://doi.org/10.1063/1.5120967
Submitted: 22 July 2019 . Accepted: 04 October 2019 . Published Online: 25 October 2019

C. Zucchetti, M. Bollani, G. Isella, M. Zani, M. Finazzi, and F. Bottegoni

Doping dependence of the electron spin diffusion length in germanium

Cite as: APL Mater. 7, 101122 (2019); doi: 10.1063/1.5120967
Submitted: 22 July 2019 • Accepted: 4 October 2019 •
Published Online: 25 October 2019

C. Zucchetti,[1] M. Bollani,[2] G. Isella,[1] M. Zani,[1] M. Finazzi,[1] and F. Bottegoni[1,a)]

AFFILIATIONS

[1] LNESS-Dipartimento di Fisica, Politecnico di Milano, Piazza Leonardo da Vinci 32, 20133 Milano, Italy
[2] Istituto di Fotonica e Nanotecnologie IFN-CNR, Piazza Leonardo da Vinci 32, 20133 Milano, Italy

[a)] **Electronic mail:** federico.bottegoni@polimi.it

ABSTRACT

We have investigated the electron spin diffusion length at room temperature in bulk *n*-doped germanium as a function of the doping concentration. To this purpose, we exploit a nonlocal spin injection/detection scheme where spins are optically injected at the direct gap of Ge and electrically detected by means of the inverse spin-Hall effect (ISHE). By optically generating a spin population in the conduction band of the semiconductor at different distances from the spin detector, we are able to directly determine the electron spin diffusion length L_s in the Ge substrate. We experimentally observe that $L_s > 20\ \mu$m for lightly doped samples and, by taking into account the electron diffusion coefficient, we estimate electron spin lifetime values τ_s larger than 50 ns. In contrast, for heavily doped Ge substrates, the spin diffusion length decreases to a few micrometers, corresponding to $\tau_s \approx 20$ ns. These results can be exploited to refine spin transport models in germanium and reduce the experimental uncertainties associated with the evaluation of L_s from other spin injection/detection techniques.

I. INTRODUCTION

The electron spin diffusion length in semiconductors is a parameter that plays a fundamental role in the design of spintronic devices. Since spin is a nonconserved quantity, the choice of a semiconductor platform where spins can be transported and manipulated over large distances is of paramount importance. To this aim, large values of the electron spin diffusion length L_s and, consequently, of the spin lifetime τ_s are required. In this frame, Ge-based spintronics can take advantage from the inversion symmetry of the Ge lattice, which avoids the presence of the Dyakonov-Perel relaxation mechanism.[1–3] As a consequence, spin lifetimes exceeding 10 ns in lightly doped Ge samples at room temperature have been reported.[4] On the contrary, in III–V semiconductors, where such a mechanism is present,[5–7] the electron spin lifetime is limited to few nanoseconds.

Therefore, germanium and Ge-based heterostructures represent natural hosting materials, where electronic and spintronic architectures can be merged.[8–13] The room-temperature spin lifetime of electrons at the indirect gap of *n*-doped Ge has been investigated by means of several electrical spin-injection/detection schemes, such as three-terminal (3T)[10,14–16] and four-terminal (4T)[17–19] lateral spin valves and spin-pumping experiments.[20–22] In this case, the spin-related voltage as a function of the applied external magnetic field is measured exploiting the Hanle effect. However, especially for 3T-devices, the role of the surface states at the metal/semiconductor junction and the presence of the impurity-assisted tunneling magnetoresistance[23] make the evaluation of the electron spin lifetime difficult, the latter being related to other parameters, such as the interface spin-resistance, the spin mixing conductance, and the injected spin polarization, which are generally subject to non-negligible experimental uncertainties. Moreover, all these techniques commonly require *heavily* doped Ge samples since a tunneling region at the metal/semiconductor contact is needed for spin injection and detection.

Spin transport and dynamics in *undoped* Ge has been mostly studied by exploiting optical spin injection and detection techniques.[24,25] The symmetry of the Ge bandstructure around the Γ point of the Brillouin zone allows the optical generation of a spin-oriented population of electrons in the conduction band, with a maximum spin polarization $P = 50\%$, when the incident photon energy is tuned to the direct gap of Ge.[26–28] Optical spin injection

can be used also in Ge-heterostructures,[11] in particular, SiGe multiple quantum wells since the spin injection can be limited to the Ge well, exploiting the different energy bandgap between Si and Ge.

Recently, a novel nonlocal spin injection/detection scheme has been developed in semiconductor-based platforms, where spins are optically injected in the semiconductor and detected by the inverse spin-Hall effect (ISHE), taking place in a thin Pt pad deposited on top of the Ge substrate.[4] In this case, the semiconductor surface is patterned by growing a series of metal stripes and the spin injection is performed through a focused light beam, impinging on the edge of each stripe. This approach has the advantage of generating a well-localized in-plane spin polarization in Ge at correspondence with the edges of the stripes.[12] We would like to stress that the spin injection and detection efficiencies, as well as the geometry of the spin injector and ISHE detector, may affect the magnitude of the measured ISHE signal but have no influence on the determination of the spin diffusion length, as explained in Ref. 4. Indeed, the ability to independently address the spin injection and detection points with microscopic resolution makes optical spin orientation combined to ISHE detection the ideal platform to investigate spin diffusion in semiconductors.

In this work, we exploit the aforementioned architecture to determine the electron spin diffusion length at room temperature in *n*-doped Ge substrates as a function of the doping concentration. In particular, by optically injecting a spin population in the conduction band of the semiconductor at different distances from the spin detector, we can directly determine the electron spin diffusion length L_s.[4]

II. SAMPLES AND EXPERIMENTAL RESULTS

We have employed four different Ge(001) substrates: the first one is unintentionally *p*-doped, with an acceptor concentration $N_a = 3 \times 10^{15}$ cm^{-3} (sample A), whereas the other three samples are *n*-doped (with phosphorous), with a donor concentration $N_d = 2 \times 10^{15}$ (sample B), 8.2×10^{16} (sample C), and 1.2×10^{18} cm^{-3} (sample D), respectively. All the substrates have been patterned by e-beam lithography (EBL) with a staircase-shaped Pt structure, which is used to inject spins in Ge when illuminated by a light beam (see below). The thickness of this structure is 20 nm and the length of each step is 50 μm. The staircase-shaped structure is faced by a 5 nm-thick Pt pad of 200 × 50 μm^2 size, used as an ISHE detector [see Fig. 1(a)]. Two 150 nm-thick Ti/Au contacts, deposited at the edges of the Pt pad along the *x*-axis, are exploited to measure the electrical signal coming from ISHE. The Pt film has been deposited by e-beam evaporation in two steps to achieve different thicknesses for the spin injector and detector. The EBL resist has been spincoated on the Ge substrate and then exposed to the electron beam of a converted scanning electron microscope (SEM) along the designed pattern (acceleration voltage of 30 kV). For these structures, a double layer of PMMA diluted to 3.5% and 1.5% in toluene has been employed. After the exposure, the PMMA has been developed to remove the soluble exposed parts by a solution of methyl isobutyl ketone (MIBK) and isopropanol (IPA) in a 1:3 ratio. Finally, during the lift-off process, the resist has been removed with acetone.

Figure 1(b) shows the confocal microscopy setup used for the measurements. The light source consists of a continuous-wave laser delivering photons at an energy equal to 0.8 eV, resonant

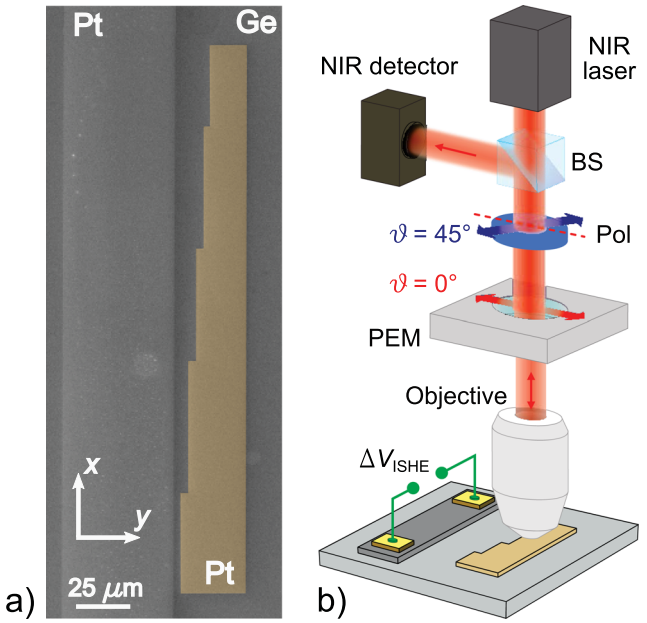

FIG. 1. (a) Scanning electron microscopy image of the Pt structures grown on sample D (doping concentration $N_d = 1.2 \times 10^{18}$ cm^{-3}). The staircase-shaped Pt structure [right-hand side in Fig. 1(a), brown-yellow] acts as spin injector, whereas the Pt rectangular pad [left-hand side of Fig. 1(a), light gray] is used as spin detector. In this case, the distances between the different steps of the spin injector and the right edge of the detector are 2.8, 6.6, 8.9, 12.3, and 15.8 μm, respectively (from bottom to top), whereas the right edges of the spin injector and detector are separated by 32.2 μm. The two Ti/Au contacts at the edges of the Pt pad are not shown in the figure. (b) Sketch of the confocal microscopy setup: the optical beam enters a beam splitter (BS), a linear polarizer (Pol), and a photoelastic modulator (PEM). Finally, it is focused on the sample by a 0.7 numerical aperture objective.

with the direct Ge bandgap at room temperature. The light enters a polarizer (Pol), a photoelastic modulator (PEM), and finally is focused on the sample by an objective with a 0.7 numerical aperture, yielding a full width at half-maximum beam size of approximately 1.5 μm. The circular polarization of the light is modulated at 50 kHz and the differential voltage signal ΔV_{ISHE} is measured between the Ti/Au contacts by a lock-in amplifier. All the measurements have been performed at room temperature.

When the focused circularly polarized light beam impinges at normal incidence on the edges of the staircase-shaped structure, the amplitude and phase of the incoming electric field are modulated so that it is possible to generate an elliptically polarized electric field in the *xz* plane of the sample.[4] In this case, dipole selection rules for direct optical transitions allow generating a spin-oriented population of electrons at the Γ point of the Ge Brillouin zone, with an in-plane spin polarization $P = 50\%$ along the *y*-axis of the sample. Therefore, by rastering the staircase-shaped structure with the focused light beam at normal incidence, we generate in the Ge conduction band spin-polarized electron populations at correspondence with the different edges of the Pt structure.[4,12] The optically injected spins diffuse in the Ge substrate and give origin to the detected ISHE signal ΔV_{ISHE} once they enter in the Pt pad.[29–33] Therefore, by measuring the ISHE signal, we are able to

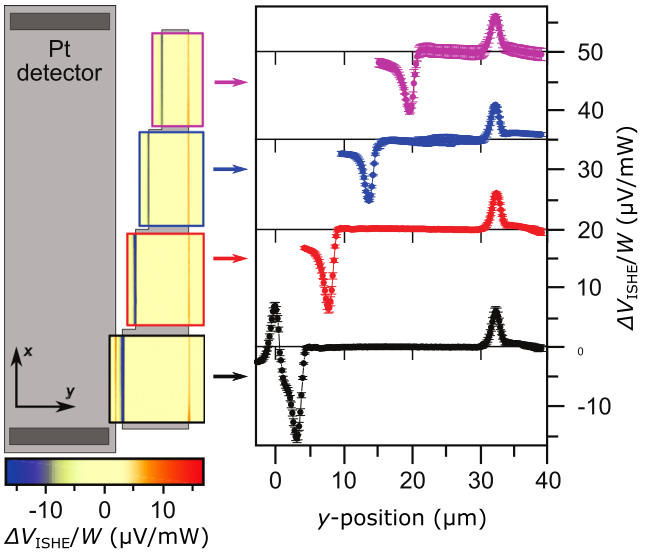

FIG. 2. ISHE map of the staircase-shaped structure for sample A (doping concentration $N_a = 3 \times 10^{15}$ cm^{-3}). The measurements have been performed with a photon energy $h\nu = 0.8$ eV and an incident power of $W = 300$ μW. The ISHE profiles corresponding to the averaged ΔV_{ISHE} along the entire length of each step (50 μm), are shown on the right. The origin of the y-axis is identified with the position of the right edge of the Pt detector.

directly measure the spin diffusion length L_s, as already pointed out in Ref. 4.

The ISHE map of sample A (Ge substrate with $N_a = 3 \times 10^{15}$ cm^{-3}) is shown in Fig. 2. The measurements have been performed with an optical power of $W = 300$ μW. Since the length of the staircase-shaped structure is larger than the maximum range of the microscope piezoelectric stage, ΔV_{ISHE}, normalized to the incident power, is only shown in the yellow boxes, corresponding to the different edges. The ISHE profiles, averaged along the entire length of each step of the structure, are shown on the right-hand side of the figure. The black profile of Fig. 2 shows a positive peak at $y = 0$, which is related to the optically injected spins at the detector edge. On the contrary, spins generated at the first step of the staircase-shaped structure results in a negative ISHE peak, as requested by the injection geometry of the pattern.[4,12] By increasing the distance between the Pt detector and the illuminated step, the amplitude of the negative peak decreases due to the finite spin diffusion length. The ISHE signal measured when the light beam is focused at $y = 32.2$ μm is due to the spins optically injected at the right edge of the staircase-shaped structure. As expected, the being latter

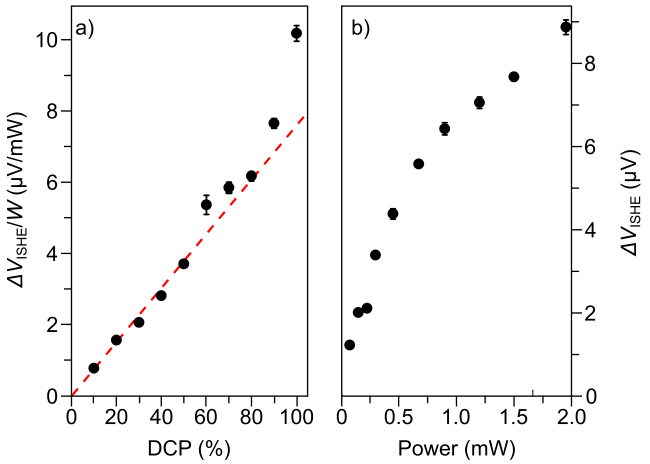

FIG. 3. Dependence of the ΔV_{ISHE} signal on (a) the degree of circular polarization (DCP) and (b) the power of the light impinging on sample A ($N_a = 3 \times 10^{15}$ cm^{-3}). The experimental points correspond to the amplitude of the ISHE signal, averaged over the entire length of the edge at distance $y = 13.8$ μm from the detector. In (a) ΔV_{ISHE} is normalized to the incident power $W = 300$ μW and the red dashed line corresponds to the linear fit of the dataset.

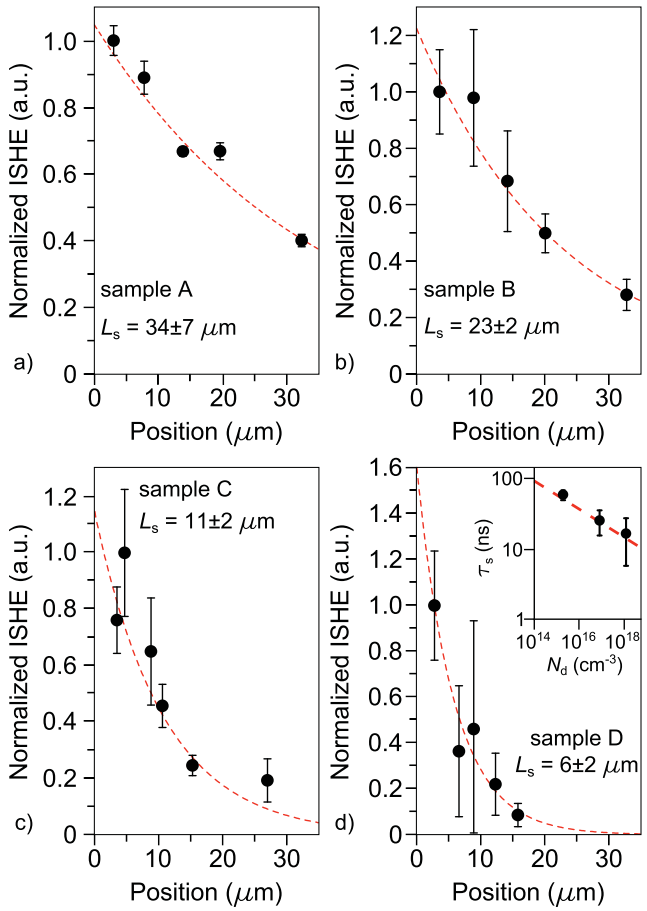

FIG. 4. ISHE signal as a function of the distance between injection and detection points for the sample (a) A ($N_a = 3 \times 10^{15}$ cm^{-3}), (b) B ($N_d = 2 \times 10^{15}$ cm^{-3}), (c) C ($N_d = 8.2 \times 10^{16}$ cm^{-3}), and (d) D ($N_d = 1.2 \times 10^{18}$ cm^{-3}). Inset: bilogarithmic plot of the estimated electron spin lifetime τ_s as a function of N_d, as obtained in Table I for samples B, C, and D. The red dashed line corresponds to the extrapolated $N_d^{-0.2}$ dependence of τ_s. The signal amplitude has been normalized to the maximum value of each dataset. Measurements have been performed with a photon energy $h\nu = 0.8$ eV and an incident power of $W = 300$ μW. The red dashed line corresponds to the exponential fit based on the unidimensional spin diffusion model.

always at the same distance from the detector, the amplitude of the corresponding ISHE peak is the same for all the profiles.[34]

To check the consistency of our measurements, we have measured the dependence of the ISHE signal from the degree of circular polarization (DCP) of the illuminating light. The experimental data for the edge of the staircase-shaped structure at $y = 13.8$ μm are reported in Fig. 3(a), where the ISHE signal has been normalized to the incident power $W = 300$ μW. As expected, ΔV_{ISHE} shows linear dependence as a function of DCP since the latter is proportional to the number of photogenerated spin polarized electrons in Ge. The power dependence of ΔV_{ISHE} [see Fig. 3(b)], measured at the same position on the sample, tends to saturate at high incident powers, according to the modulation imposed by the photovoltage across the Pt/Ge Schottky junction.[31,32]

We have then performed ISHE measurements for all the Ge substrates, by exploiting similar staircase-shaped Pt structures. The results are summarized in Fig. 4. The ISHE signal has been normalized to the maximum value for each dataset. The experimental points are obtained by averaging the ISHE signal at the corresponding injection edge over the entire length of the step.

III. DISCUSSION

The experimental data of Fig. 4 can be interpreted in the frame of a unidimensional spin diffusion model:[4,5,31,35,36] in this case, $\Delta V_{ISHE} \propto e^{-y/L_s}$, where $L_s = \sqrt{D_e \tau_s}$ is the spin diffusion length, with D_e being the electron diffusion coefficient. Since the ISHE signal is acquired as a function of the distance between the injection and detection points, the relative variation of the signal can only be ascribed to the spin depolarization. Therefore, it is possible to employ the ΔV_{ISHE} dependence upon y to fit the experimental datasets of Fig. 4 and estimate L_s, which is the only free parameter that needs to be determined by fitting. For low doping levels, corresponding to sample A and B, we obtain the extremely large values $L_s = 34 \pm 7$ μm and 23 ± 2 μm, respectively. For the heavily doped Ge substrates, i.e., sample C and D, the spin diffusion length decreases, and we estimate $L_s = 11 \pm 2$ μm and 6 ± 2 μm, respectively, in agreement with the results reported in Ref. 4.

It is important to note that when the light beam impinges on the edge of the staircase-shaped structure, a photovoltage is generated between the injection and the detection point,[37] resulting in a photoinduced electric field E_{ph} along the direction of spin diffusion. The latter might create a drift spin current that could affect our estimation of the electron spin diffusion length, as explained, for instance, in Ref. 38. However, spin transport associated with drift currents becomes relevant when the amplitude of E_{ph} is larger than $\approx 10^4$ V/m. To rule this mechanism out, we have estimated E_{ph} for all the samples by measuring the photoinduced voltage between the Pt spin injector and detector, when each step of the staircase-shaped Pt structure was illuminated. We have found $E_{ph} < 10^2$ V/m in all cases, indicating that the photovoltage cannot give any sizeable contribution to the spin transport and hence have no influence on the measured L_s values. Possible artefacts on the estimation of the spin diffusion length due the nonuniform illumination of the sample can also be ruled out since all the measurements have been performed with an incident power lying in a power range where the ISHE signal is linear with respect to W. This is the expected behavior in a diffusion regime where temperature gradients can be neglected.

TABLE I. From the left to the right: sample code, electron spin diffusion length L_s, electron diffusion coefficient D_e from Ref. 39, electron spin lifetime τ_s, estimated from the L_s values in the second column, and electron spin lifetime τ_s^{th}, calculated from the spin relaxation cross sections reported in Refs. 41, 44, and 45.

Sample (cm^{-3})	L_s (μm)	D_e (cm^2/s)	τ_s (ns)	τ_s^{th} (ns)
A: $N_a = 3 \times 10^{15}$	34 ± 7	87	132 ± 61	4.8
B: $N_d = 2 \times 10^{15}$	23 ± 2	87	60 ± 10	4.8
C: $N_d = 8.2 \times 10^{16}$	11 ± 2	45	26 ± 10	2.5
D: $N_d = 1.2 \times 10^{18}$	6 ± 2	21	17 ± 11	0.5

The experimental results are summarized in Table I. By taking into account D_e, extracted from the mobility measurements of Ref. 39, we can also give an estimation of the electron spin lifetime τ_s. Direct estimations of L_s in undoped Ge are not available in the literature because electrical spin injection/detection schemes require heavily doped Ge substrates to achieve a thin depleted region at the metal/semiconductor contacts. Therefore, the comparison between our L_s values and those reported in the literature is only meaningful for high doping levels. In this case, the estimation of L_s for sample D in Table I is in agreement with the one reported in Ref. 10, whereas it is larger than what observed in Refs. 21 and 22.

In the past years, experimental investigations of spin-related properties in Ge have been mainly performed by means of the Hanle effect in 3T- and 4T-devices, from which it is possible to estimate the electron spin lifetime τ_s.[14–20] The τ_s values thus obtained, however, are considerably smaller than those that we infer from L_s in this work for similar doping concentrations. This is true both for lightly and heavily doped Ge substrates, where 3T-measurements estimate $\tau_s < 1$ ns[16] and $0.3 < \tau_s < 0.7$ ns,[40] respectively. In this sense, since the role of the spin-dependent tunneling in 3T devices is still debated, whereas our estimation of L_s does not depend on any other parameter involved in the measurement, the comparison between the experimental results of Refs. 10 and 14–21 and those of Table I could help clarifying the mechanism of spin injection and extraction at the metal/semiconductor interfaces.

Nevertheless, it is worth noticing that the estimation of τ_s for a n-doped Ge sample by means of optical techniques, reported in Ref. 41, is consistent with the one obtained in Table I for sample D.

Moreover, it has been theoretically proposed[42] and experimentally observed[43] that for heavily n-doped semiconductors the spin-polarized electron diffusion coefficient can significantly differ from that of unpolarized carriers, especially at low temperature. In our case, this phenomenon could be significant only for sample D and could affect the estimation of the electron spin lifetime, by reducing τ_s at most by a factor two.

Finally, we have theoretically estimated the electron spin lifetime from spin relaxation cross sections[41,44,45] (see the last column of Table I). The circularly polarized light generates around the Γ point of the Ge Brillouin zone a spin-oriented population of electrons,

which is rapidly relaxed toward the L minima. Since the energy relaxation occurs in a time scale much lower than the one characteristic for spin depolarization,[46] it is possible to assume that the electrons are transferred to the indirect Ge gap without losing their spin polarization. At the L minima, spins can relax due to the intra- and intervalley scattering as well as impurity-driven scattering, depending on the doping concentration. For samples A and B, we have considered only intra- and intervalley spin relaxation mechanisms, obtaining $\tau_s^{th} \approx 5$ ns, which is much lower than the value extrapolated from our experimental measurements, but in agreement with the well-established calculations of Ref. 44, whereas, for samples C and D, we have also taken into account the impurity-assisted spin relaxation mechanism.[7,41,46] Recently, a detailed calculations on impurity-driven spin relaxation mechanisms in multivalley semiconductors has been proposed in Ref. 47, suggesting that the electron spin lifetime should follow a $N_d^{-\frac{4}{3}}$ dependence as a function of the n-type doping concentration N_d. Although this has been experimentally verified in degenerate n-Ge by means of electrical measurements on lateral spin valves at low temperatures,[22] our experimental data rather indicate a $N_d^{-0.2}$ dependence on N_d, as shown in the inset of Fig. 4(d). Such a discrepancy could be phenomenologically justified by the fact that at room temperature and in the investigated doping range, especially for samples B and C, spins are mostly depolarized through intervalley spin relaxation promoted by phonons, as suggested in Refs. 44 and 45. All the calculations appear to underestimate the electron spin lifetime in Ge for at least an order of magnitude, as already suggested in Ref. 4, so our measurements can be exploited to better calibrate the parameters involved in the models describing spin-related intervalley scattering at the L minima of Ge.

In conclusion, we have determined the electron spin diffusion length in bulk n-Ge by means of a nonlocal spin injection/detection scheme. By varying the distance between the spin injection and detection point, we are able to estimate the electron spin diffusion length as a function of the doping concentration without any supplemental parameter. Taking into account the large discrepancies between our experimental data and the ones already reported in the literature for similar systems, these results can be exploited to eventually refine spin transport and diffusion models in germanium and reduce the experimental uncertainties associated with the evaluation of the spin diffusion length L_s from other spin injection/detection techniques.

REFERENCES

[1] *Optical Orientation*, Modern Problems in Condensed Matter Sciences Vol. 8, edited by F. Meier and B. P. Zakharchenya (Elsevier, Amsterdam, 1984).
[2] F. Bottegoni, H.-J. Drouhin, G. Fishman, and J.-E. Wegrowe, Phys. Rev. B **85**, 235313 (2012).
[3] F. Bottegoni, H.-J. Drouhin, J.-E. Wegrowe, and G. Fishman, J. Appl. Phys. **111**, 07C305 (2012).
[4] C. Zucchetti, F. Bottegoni, C. Vergnaud, F. Ciccacci, G. Isella, L. Ghirardini, M. Celebrano, F. Rortais, A. Ferrari, A. Marty, M. Finazzi, and M. Jamet, Phys. Rev. B **96**, 014403 (2017).
[5] I. Zutić, J. Fabian, and S. Das Sarma, Rev. Mod. Phys. **76**, 323 (2004).
[6] N. Stern, S. Ghosh, G. Xiang, M. Zhu, N. Samarth, and D. Awschalom, Phys. Rev. Lett. **97**, 126603 (2006).
[7] F. Bottegoni, A. Ferrari, G. Isella, M. Finazzi, and F. Ciccacci, Phys. Rev. B **88**, 121201 (2013).
[8] D. J. Paul, Adv. Mater. **11**, 191 (1999).
[9] R. Soref, Nat. Photonics **4**, 495 (2010).
[10] A. Jain, J.-C. Rojas-Sanchez, M. Cubukcu, J. Peiro, J. Le Breton, E. Prestat, C. Vergnaud, L. Louahadj, C. Portemont, C. Ducruet, V. Baltz, A. Barski, P. Bayle-Guillemaud, L. Vila, J.-P. Attané, E. Augendre, G. Desfonds, S. Gambarelli, H. Jaffrès, J.-M. George, and M. Jamet, Phys. Rev. Lett. **109**, 106603 (2012).
[11] F. Pezzoli, F. Bottegoni, D. Trivedi, F. Ciccacci, A. Giorgioni, P. Li, S. Cecchi, E. Grilli, Y. Song, M. Guzzi, H. Dery, and G. Isella, Phys. Rev. Lett. **108**, 156603 (2012).
[12] F. Bottegoni, M. Celebrano, M. Bollani, P. Biagioni, G. Isella, F. Ciccacci, and M. Finazzi, Nat. Mater. **13**, 790 (2014).
[13] F. Bottegoni, C. Zucchetti, S. Dal Conte, J. Frigerio, E. Carpene, C. Vergnaud, M. Jamet, G. Isella, F. Ciccacci, G. Cerullo, and M. Finazzi, Phys. Rev. Lett. **118**, 167402 (2017).
[14] K.-R. Jeon, B.-C. Min, Y.-H. Jo, H.-S. Lee, I.-J. Shin, C.-Y. Park, S.-Y. Park, and S.-C. Shin, Phys. Rev. B **84**, 165315 (2011).
[15] K.-R. Jeon, B.-C. Min, Y.-H. Park, H.-S. Lee, C.-Y. Park, Y.-H. Jo, and S.-C. Shin, Appl. Phys. Lett. **99**, 162106 (2011).
[16] A. Hanbicki, S.-F. Cheng, R. Goswami, O. van 't Erve, and B. Jonker, Solid State Commun. **152**, 244 (2012).
[17] F. Rortais, C. Vergnaud, A. Marty, L. Vila, J.-P. Attané, J. Widiez, C. Zucchetti, F. Bottegoni, H. Jaffrès, J.-M. George, and M. Jamet, Appl. Phys. Lett. **111**, 182401 (2017).
[18] M. Yamada, M. Tsukahara, Y. Fujita, T. Naito, S. Yamada, K. Sawano, and K. Hamaya, Appl. Phys. Express **10**, 093001 (2017).
[19] K. Hamaya, Y. Fujita, M. Yamada, M. Kawano, S. Yamada, and K. Sawano, J. Phys. D: Appl. Phys. **51**, 393001 (2018).
[20] J.-C. Rojas-Sánchez, M. Cubukcu, A. Jain, C. Vergnaud, C. Portemont, C. Ducruet, A. Barski, A. Marty, L. Vila, J.-P. Attané, E. Augendre, G. Desfonds, S. Gambarelli, H. Jaffrès, J.-M. George, and M. Jamet, Phys. Rev. B **88**, 064403 (2013).
[21] S. Dushenko, M. Koike, Y. Ando, T. Shinjo, M. Myronov, and M. Shiraishi, Phys. Rev. Lett. **114**, 196602 (2015).
[22] M. Yamada, Y. Fujita, M. Tsukahara, S. Yamada, K. Sawano, and K. Hamaya, Phys. Rev. B **95**, 161304 (2017).
[23] O. Txoperena, Y. Song, L. Qing, M. Gobbi, L. E. Hueso, H. Dery, and F. Casanova, Phys. Rev. Lett. **113**, 146601 (2014).
[24] C. Guite and V. Venkataraman, Phys. Rev. Lett. **107**, 166603 (2011).
[25] A. Giorgioni, E. Vitiello, E. Grilli, M. Guzzi, and F. Pezzoli, Appl. Phys. Lett. **105**, 152404 (2014).
[26] R. Allenspach, F. Meier, and D. Pescia, Phys. Rev. Lett. **51**, 2148 (1983).
[27] F. Bottegoni, G. Isella, S. Cecchi, and F. Ciccacci, Appl. Phys. Lett. **98**, 242107 (2011).
[28] F. Bottegoni, A. Ferrari, G. Isella, S. Cecchi, M. Marcon, D. Chrastina, G. Trezzi, and F. Ciccacci, J. Appl. Phys. **111**, 063916 (2012).
[29] E. Saitoh, M. Ueda, H. Miyajima, and G. Tatara, Appl. Phys. Lett. **88**, 182509 (2006).
[30] J. Sinova, S. O. Valenzuela, J. Wunderlich, C. H. Back, and T. Jungwirth, Rev. Mod. Phys. **87**, 1213 (2015).
[31] G. Isella, F. Bottegoni, A. Ferrari, M. Finazzi, F. Ciccacci, G. Isella, F. Bottegoni, A. Ferrari, M. Finazzi, and F. Ciccacci, Appl. Phys. Lett. **106**, 232402 (2015).
[32] F. Bottegoni, A. Ferrari, F. Rortais, C. Vergnaud, A. Marty, G. Isella, M. Finazzi, M. Jamet, and F. Ciccacci, Phys. Rev. B **92**, 214403 (2015).
[33] F. Bottegoni, C. Zucchetti, G. Isella, E. Pinotti, M. Finazzi, and F. Ciccacci, J. Appl. Phys. **124**, 033902 (2018).
[34] Note that the amplitude of the ISHE signal, related to optical spin injection at the right edge of the Pt detector, cannot be straighforwardly compared to the ISHE amplitude obtained when illuminating the staircase-shaped structure since the thickness of the two Pt structures is very different.
[35] J. Fabian, A. Matos-Abiague, C. Ertler, P. Stano, and I. Žutić, Acta Physica Slovaca **57**(4-5), 565–907 (2007).
[36] A. Spiesser, H. Saito, Y. Fujita, S. Yamada, K. Hamaya, S. Yuasa, and R. Jansen, Phys. Rev. Appl. **8**, 064023 (2017).

[37] F. Bottegoni, C. Zucchetti, F. Ciccacci, M. Finazzi, and G. Isella, Appl. Phys. Lett. **110**, 042403 (2017).
[38] Z. Yu and M. Flatté, Phys. Rev. B **66**, 235302 (2002).
[39] V. I. Fistul, M. Iglitsyn, and E. M. Omelyanovskii, Sov. Phys. Solid State **4**, 784 (1962).
[40] K. Kasahara, Y. Baba, K. Yamane, Y. Ando, S. Yamada, Y. Hoshi, K. Sawano, M. Miyao, and K. Hamaya, J. Appl. Phys. **111**, 07C503 (2012).
[41] C. Guite and V. Venkataraman, Appl. Phys. Lett. **101**, 252404 (2012).
[42] M. E. Flatte and J. M. Byers, Phys. Rev. Lett. **84**, 4220 (2000).
[43] J. Kikkawa and D. D. Awschalom, Nature **397**, 139 (1999).
[44] T. Yu and M. W. Wu, J. Phys.: Condens. Matter **27**, 255001 (2015).
[45] P. Li, Y. Song, and H. Dery, Phys. Rev. B **86**, 085202 (2012).
[46] C. Zucchetti, F. Bottegoni, G. Isella, M. Finazzi, F. Rortais, C. Vergnaud, J. Widiez, M. Jamet, and F. Ciccacci, Phys. Rev. B **97**, 125203 (2018).
[47] Y. Song, O. Chalaev, and H. Dery, Phys. Rev. Lett. **113**, 167201 (2014).